

# Ionic Liquid Crystals Formed by Self-Assembly around an Anionic Anthracene Core

Jean-Hubert Olivier,<sup>[a]</sup> Franck Camerel,<sup>\*[a]</sup> Joaquín Barberá,<sup>[b]</sup> Pascal Retailleau,<sup>[c]</sup> and Raymond Ziessel<sup>\*[a]</sup>

**Abstract:** We have designed and synthesised a series of modular, mesogenic complexes based on anthracene-2,6-disulfonate and trialkoxybenzyl-functionalised imidazolium cations. Each complex contains a central, rigid, dianionic anthracene core and two flexible monocations bearing paraffin chains anchored on imidazolium rings. Anthracene-2,6-disulfonate can be crystallised with various simple alkylammonium ions and, in the case of  ${}^+\text{N}(\text{CH}_3)_2(\text{C}_{16}\text{H}_{33})_2$ , a crystal structure determina-

tion has shown that the long paraffinic chains are intercalated between the anthracene moieties. The dianion forms columnar mesophases with trialkoxybenzylimidazolium cations, as identified by polarising optical microscopy and X-ray scattering measurements. Differential scanning calorimetry stud-

**Keywords:** anthracene • liquid crystals • self-assembly • luminescence • mesophases

ies confirmed mesomorphic behaviour from room temperature to about 200 °C for alkyl chains containing 8, 12 and 16 carbon atoms. The strong luminescence of anthracene is maintained in the mesophase and fluorescence measurements confirmed the presence of *J* aggregates in all cases. The new functional materials described herein provide an easy access to stable and luminescent mesomorphic materials engineered by an ionic self-assembly process.

## Introduction

Supramolecular chemistry leading to nanosegregation processes is a sophisticated tool for the design of new functional liquid crystalline materials.<sup>[1]</sup> The design of  $\pi$ -conjugated liquid crystals is particularly appealing due to their possible applications in electrochemical devices.<sup>[2]</sup> Of especial interest is their use as active components in solar cells because some can carry charges and excitons more efficiently than conjugated polymers.<sup>[3]</sup> Luminescent  $\pi$ -conjugated liquid

crystals have also been found to be interesting candidates for the preparation of organic light-emitting diodes (OLEDs) in which light is generated by electrical excitation.<sup>[4]</sup>

In the family of  $\pi$ -conjugated acene units,<sup>[5]</sup> the anthracene nucleus, which has a high fluorescence quantum yield, is of particular interest. Thus, anthracene derivatives have been used in chemiluminescent formulations,<sup>[6]</sup> as molecular probes,<sup>[7]</sup> in OLEDs<sup>[8]</sup> and in organic field-effect transistors (OFETs).<sup>[9]</sup> The electronic performance in such organic electronic devices strongly relies on intermolecular order in the solid state. With liquid crystalline materials, anisotropic intermolecular ordering can be finely tuned by appropriate functionalisation and shaping of the molecules. The manifestation of mesomorphic properties in  $\pi$ -conjugated molecules is not easy to guarantee, however, and large numbers of chemical modifications are usually necessary to obtain the desired properties. This is probably the reason why, despite the remarkable photophysical and -chemical properties of anthracene, very few attempts have been made to prepare mesogenic derivatives and to embed them in optoelectronic devices.<sup>[10]</sup>

A simple way to avoid tedious synthetic modifications and to easily produce mesomorphic materials is to use the recently developed ionic self-assembly (ISA) process,<sup>[11]</sup> a

[a] J.-H. Olivier, Dr. F. Camerel, Dr. R. Ziessel  
Laboratoire de Chimie Organique et Spectroscopies Avancées (LCOSA)  
Ecole Européenne de Chimie, Polymères et Matériaux, CNRS  
25 rue Becquerel, 67087 Strasbourg Cedex 02 (France)  
fcamerel@chimie.u-strasbg.fr  
E-mail: ziessel@unistra.fr

[b] Dr. J. Barberá  
Liquid Crystal Group, Departamento de Química Orgánica  
Instituto de Ciencia de Materiales de Aragón  
Universidad de Zaragoza-CSIC, 50009 Zaragoza (Spain)

[c] Dr. P. Retailleau  
Laboratoire de Cristalochimie, ICSN—CNRS  
Bât 27 1 avenue de la Terrasse, 91198 Gif-sur-Yvette, Cedex (France)

Supporting information for this article is available on the WWW under <http://dx.doi.org/10.1002/chem.200900721>.

technique in which multiple charged organic species are organised by their association with oppositely charged amphiphilic counterions. Hierarchical superstructures can then be

**Abstract in French:** Une nouvelle série de complexes mésogènes obtenus par association électrostatique entre l'anthracène-2,6-disulfonate et des imidazoliums fonctionnalisés a été synthétisée. Les propriétés optiques et d'auto-organisation de ces complexes, constitués d'un noyau rigide central dianionique d'anthracène et de deux cations flexibles à cœur imidazolium, ont été étudiées. Associé à des dérivés d'ammoniums portant de longues chaînes carbonées, l'anthracène-2,6-disulfonate peut être cristallisé et la structure obtenue avec la cation  ${}^+\text{N}(\text{CH}_3)_2(\text{C}_{16}\text{H}_{33})_2$  montre qu'il n'y a pas de ségrégation entre les chaînes grasses et le cœur rigide du dérivé d'anthracène. Par contre, associé à des imidazoliums fonctionnalisés par des dérivés tris-alkoxybenzyl, une micro-ségrégation peut être engendrée et des mésophases colonnaires ont pu être observées et identifiées par POM ainsi que par diffraction aux rayons X. Des études par calorimétrie différentielle à balayage (DSC) confirme le comportement mésomorphe des complexes sur une large gamme de température s'étalant de 20°C à 200°C avec des chaînes alkyles à 8, 12, 16 atomes de carbone. Les propriétés de luminescence de l'anthracène sont maintenues au sein des mésophases et des études par spectroscopie d'émission confirment la présence d'agrégat de type J entre les fragments aromatiques. Ces nouveaux complexes fonctionnels, obtenus par auto-assemblage par voie électrostatique, fournissent un accès rapide et simple à des matériaux mésomorphes et luminescents.

**Abstract in Spanish:** Hemos diseñado y sintetizado una serie de complejos mesógenos modulares basados en antraceno-2,6-disulfonato y cationes imidazolio funcionalizados con tris(alcoxi)encilo. Todos los complejos contienen un núcleo central rígido dianiónico de antraceno y dos monocaciones flexibles que portan cadenas parafínicas ancladas en los anillos de imidazol. El antraceno-2,6-disulfonato puede cristalizarse con varios iones alquilamonio simples y, en el caso de  ${}^+\text{N}(\text{CH}_3)_2(\text{C}_{16}\text{H}_{33})_2$ , la determinación de la estructura cristalina ha mostrado que las cadenas parafínicas largas están intercaladas entre las unidades de antraceno. Con los cationes tris(alcoxi)encilimidazolio, el dianión forma mesofases columnares identificadas por medidas de microscopía óptica con luz polarizada y difracción de rayos X. Los estudios de DSC confirman el comportamiento mesomorfo desde temperatura ambiente hasta 200°C para cadenas alquílicas que contienen 8, 12 y 16 átomos de carbono. La fuerte luminiscencia del antraceno se mantiene en la mesofase y las medidas de fluorescencia confirman la presencia de agregados J en todos los casos. Los nuevos materiales funcionales descritos aquí representan un fácil acceso a materiales mesomorfos luminiscentes estables generados por un proceso de auto-ensamblaje iónico.

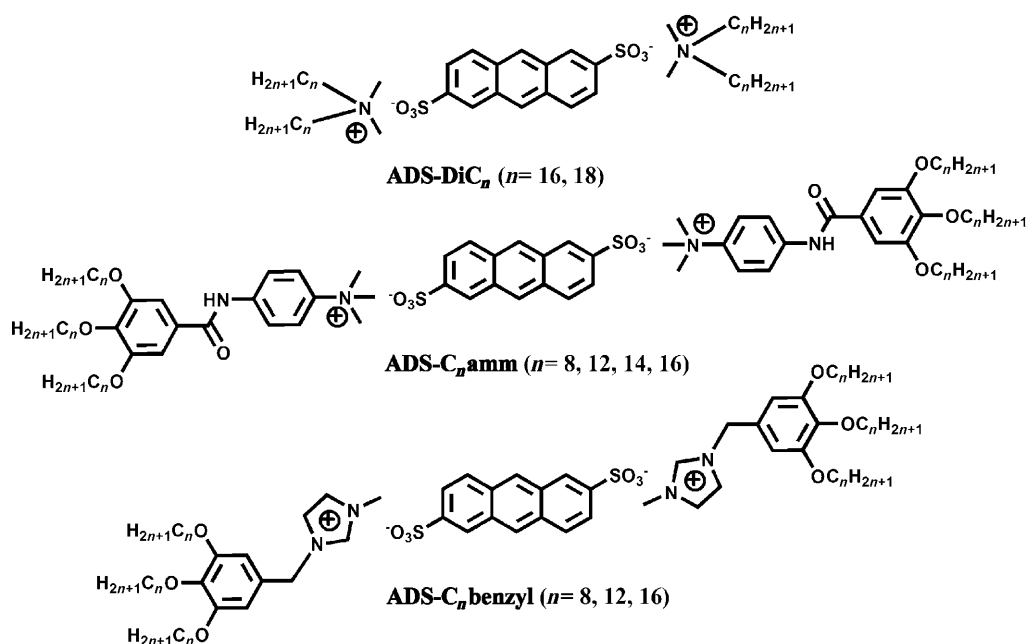
generated in an ISA process by the electrostatic interactions between charged amphiphiles and oppositely charged oligoelectrolytes as the primary interaction and by hydrophobic and  $\pi$ - $\pi$  interactions as the secondary interactions in the self-organisation process. Additional interactions, such as hydrogen-bonding, can also be introduced to further stabilise and control the organisation of the assemblies.<sup>[12]</sup> This process (for the construction of liquid-crystalline materials based on stepwise non-covalent interactions) allows easy tuning of the properties of the emergent structures by the careful choice of the alkyl volume fraction (internal solvent) by simple exchange of the binding partner in the corresponding assembly step without tedious synthetic operations.

Standard, commercially available, charged surfactants are commonly used and some more elaborate amphiphilic molecules that introduce new functionalities, such as hydrogen-bonding, chirality or polymerisable groups inside the ISA materials, have been developed.<sup>[13]</sup> In most of the amphiphilic binding partners used in the cited ISA processes, the positive charge is localised on ammonium or phosphonate polar head-groups and, to the best of our knowledge, no organic functions with delocalised charge, such as an imidazolium fragment, have been used in the ionic self-assembly process to organise a negatively charged functional core.

In this report we describe ISA processes involving a dianionic anthracene derivative and both simple alkylammonium amphiphiles and mesogenic imidazolium species. The aim of this work was to organise a luminescent  $\pi$ -conjugated fragment into columnar liquid-crystalline materials. For this purpose, commercially available double-tailed ammonium surfactants and synthetic wedge-shaped amphiphilic molecules with ammonium groups at the tip,<sup>[14]</sup> known to be able to organise charged molecules into mesogenic materials through ISA processes, were selected as counterions. A series of imidazolium cations carrying trialkoxyphenyl moieties of various chain lengths, described earlier by Kato and co-workers,<sup>[15]</sup> was also selected, as these molecules are known to form columnar mesophases over wide temperature ranges including room temperature. The idea was to check the capacity of these mesogenic cations to generate liquid-crystalline behaviour when in association with an anionic anthracene derivative. The luminescence of the mesophases duly obtained has been investigated in both the liquid and solid states to evaluate the nature of the intermolecular interactions engendered in the crystalline and mesomorphic states.

## Results and Discussion

**Synthesis:** The chemical structures of the ISA complexes are depicted in Scheme 1. Double-tail dialkyldimethylammonium bromide surfactants (**DiC<sub>n</sub>**,  $n = 16, 18$ ) were purchased from Aldrich and used as received without further purification. The synthetic ammonium amphiphiles **C<sub>n</sub>amm** with iodide as the counterion were synthesised in good yields as



Scheme 1.

previously described by the reaction of 3,4,5-tri-*n*-alkoxybenzoic acid chlorides ( $n=8, 12, 14, 16$ ) with *N,N*-dimethyl-1,4-phenylenediamine dihydrochloride in dry dichloromethane in the presence of triethylamine followed by alkylation in iodomethane at reflux.<sup>[14]</sup> The 1-methyl-3-(3,4,5-trialkoxybenzyl)imidazolium chlorides (**[C<sub>n</sub>benzyl]<sup>+</sup>Cl<sup>-</sup>**) were synthesised as previously described by the reaction of 1-methylimidazole and the corresponding 3,4,5-trialkoxybenzyl chlorides ( $n=8, 12, 16$ ) in toluene at 80 °C overnight.<sup>[15]</sup> Anthracene-2,6-disulfonic acid with potassium as the counterion (**ADS-K**) was prepared according to a published procedure.<sup>[16]</sup>

The ion associate complexes formed between the anthracene-2,6-disulfonate anion and the various ammonium and imidazolium cations were obtained by cation metathesis. The complexation was performed in DMF and the complexes isolated by precipitation with water. The ammonium complexes were recrystallised from a dichloromethane/acetonitrile mixture by slow evaporation of CH<sub>2</sub>Cl<sub>2</sub> whereas the imidazolium complexes were recrystallised from hot DMSO. Complexation in a 2:1 ratio was con-

firmed in all cases by elemental analysis and NMR spectroscopy. In particular, the proton signal at 6.77 ppm, characteristic of the aromatic protons of the trialkoxybenzyl substituents, has twice the intensity of the anthracene signals at 7.68, 8.01, 8.26 and 8.60 ppm. The <sup>1</sup>H NMR spectrum of the **ADS-C<sub>12</sub>benzyl** species is given in Figure 1 as a representative case.

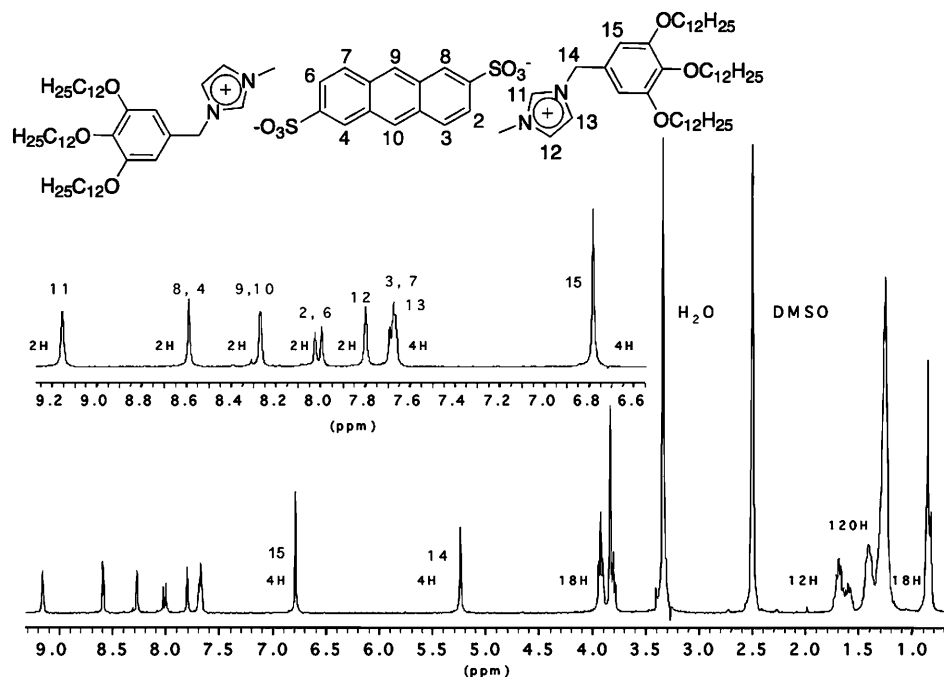


Figure 1. <sup>1</sup>H NMR spectrum of **ADS-C<sub>12</sub>benzyl** in [D<sub>6</sub>]DMSO at room temperature, including peak assignments and their integrals.

**Molecular structure of ADS-DiC<sub>16</sub> by single-crystal X-ray diffraction:** Single crystals of ADS-DiC<sub>16</sub> suitable for X-ray diffraction were obtained by slow evaporation from a CH<sub>2</sub>Cl<sub>2</sub>/CH<sub>3</sub>CN solvent mixture. This compound crystallises in the triclinic space group *P* $\bar{1}$  (*a*=9.832(5), *b*=16.397(7), *c*=28.147(9) Å,  $\alpha$ =73.52(4),  $\beta$ =81.93(3),  $\gamma$ =78.01(3)°, *V*=4240.31(300) Å<sup>3</sup>, *Z*=2). Figure 2 shows the structure of

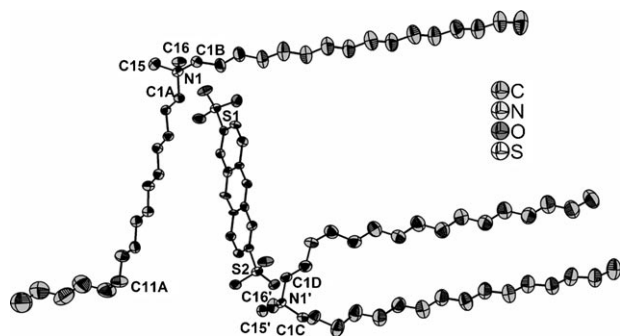


Figure 2. ORTEP view of the ADS-DiC<sub>16</sub> complex with the principal atomic numbering (thermal ellipsoids at the 50% probability level). Selected bond lengths [Å] and angles [°]: N1–C15 1.506(32), N1–C16 1.516(30), N1–C1B 1.518(17), N1–C1A 1.521(16); C15–N1–C16 106.49(55), C15–N1–C1B 107.33(64), C16–N1–C1B 111.3(6), C15–N1–C1A 110.44(61), C16–N1–C1A 111.01(62), C1B–N1–C1A 110.15(63), N1'–C15' 1.490(25), N1'–C16' 1.507(31), N1'–C1C 1.506(38), N1'–C1D 1.524(24); C15'–N1'–C16' 108.90(58), C15'–N1'–C1C 112.24(62), C16'–N1'–C1C 107.28(65), C15'–N1'–C1D 108.44(63), C16'–N1'–C1D 108.92(63), C1C–N1'–C1D 110.98(62).

ADS-DiC<sub>16</sub> as well as the atomic numbering and labelling scheme. The asymmetric unit contains one anthracene-2,6-disulfonate dianionic molecule and two ammonium DiC<sub>16</sub> cations in general positions (not localised on a symmetry element). The X-ray crystal structure confirms the 2:1 stoichiometric ratio determined by NMR and elemental analysis. The anthracene fragment is completely planar and the substitutions at the 2- and 6-positions are also confirmed. In one of the ammonium cations, the two long carbon chains appear to be almost parallel and fully extended. In contrast, in the other ammonium fragment, the two long carbon chains point in opposite directions and one chain has a strong bend at the eleventh carbon atom (C1–C11–C16=117.12°). The nitrogen atoms are tetrahedral and the C–N distances are almost identical.

A projection of the crystalline structure along the *b* axis is presented in Figure 3. The crystalline network can be described as being constructed of alternate layers of long carbon chains and anthracene units stacked along the *c* axis. The crystalline arrangement has some similarities with the molecular organisation of a smectic phase. Segregation between the rigid aromatic part and the flexible carbon chains seems to govern the molecular organisation, although charge association must also have an influence. A close look at the crystalline structure reveals that the bent carbon chains (see the ORTEP view in Figure 2) carried by one of the ammonium cations are stacked between the anthracene

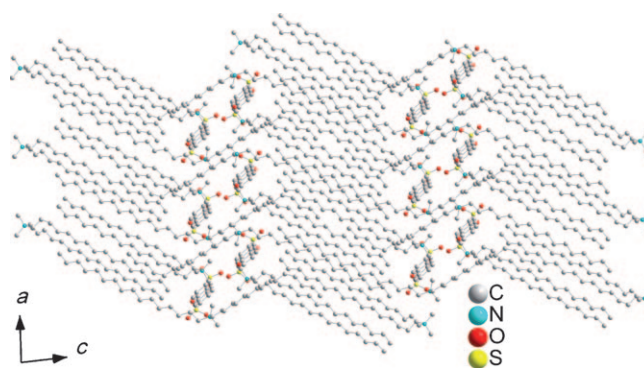


Figure 3. Projection of the crystalline structure of the ADS-DiC<sub>16</sub> complex along the *b* axis (hydrogen atoms have been omitted for clarity).

molecules. The anthracene units do not interact or form aggregated species in the crystal structure and the fluorophores are completely isolated within the layered system. Crystalline salts of anthracene-2,6-disulfonate and single-tail ammonium surfactants (CH<sub>3</sub>(CH<sub>2</sub>)<sub>*n*</sub>NH<sub>3</sub><sup>+</sup>; *n*=0–4) have already been reported and it has been demonstrated that the nature of the aggregated anthracene species as well as their photophysical properties depend on the length of the carbon chains.<sup>[17]</sup> In these previous studies, in which short carbon chains were used (*n*=0–4), it was shown that an increase in the length of the alkyl chains led to a decrease in the dimensionality of the anthracene arrangements from 2D to 1D. The present structure, in which a 0D arrangement of anthracene cores is observed, extends these previous observations.

**Optical properties in solution:** The spectroscopic data for the ADS complexes in dilute solution are gathered in Table 1. ADS-C<sub>12</sub>amm, ADS-C<sub>14</sub>amm and ADS-C<sub>16</sub>amm were found to be poorly soluble in dichloromethane. The absorption spectra of the ADS-K salt in water and of the ADS derivatives in dichloromethane and in DMF show three main absorption bands centred around 341, 358 and 378 nm (see Figure 4 as a typical example), characteristic of the vibronic spectrum of anthracene. The positions and intensities of the absorption bands are not affected by the nature of the solvent or the counterion (Table 1).

Excitation at 358 nm leads to a broad structured emission band extending from 370 to 550 nm and displaying maxima at around 396, 415 and 440 nm (Table 1 and Figure 4). The fluorescence spectrum shows relatively good mirror symmetry for the lowest-energy absorption transitions, which confirms that these transitions are weakly polarised and originate from the same state, typical of singlet emitters. The weak Stokes shifts observed are in good agreement with a singlet emitting state and the excitation spectra perfectly match the absorption spectra, which is in keeping with a unique excited state. The parameter that is strongly dependent upon the nature of the solvent is the quantum yield, which decrease from 47% in water to about 15–20% in DMF and about 7% in dichloromethane. However, the quantum yields measured in a given solvent do not depend

Table 1. Optical data measured in solution at 298 K.

	Solvent	$\lambda_{\text{abs}}$ [nm]	$\epsilon$ [ $\text{M}^{-1}\text{cm}^{-1}$ ]	$\lambda_{\text{F}}$ [nm]	$\Phi_{\text{F}}$ [a]
<b>ADS-K</b>	water	382	3885	397	0.47
		361	4120	419	
		335	3650	445	
<b>ADS-K</b>	DMF	377	3800	394	0.13
		358	5090	416	
		341	4120	440	
<b>ADS-DiC<sub>16</sub></b>	CH <sub>2</sub> Cl <sub>2</sub>	378	3940	396	0.08
		358	5400	416	
		341	4580	440	
<b>ADS-DiC<sub>18</sub></b>	CH <sub>2</sub> Cl <sub>2</sub>	378	4140	395	0.07
		358	5570	416	
		342	4140	441	
<b>ADS-C<sub>8</sub>amm</b>	CH <sub>2</sub> Cl <sub>2</sub>	379	4580	398	0.06
		360	5990	418	
		343	5020	442	
<b>ADS-C<sub>8</sub>amm</b>	DMF	376	3000	399	0.21
		358	4130	416	
		341	3330	440	
<b>ADS-C<sub>12</sub>amm</b>	DMF	377	3590	396	0.17
		358	4890	415	
		341	3990	441	
<b>ADS-C<sub>14</sub>amm</b>	DMF	376	4010	394	0.15
		358	5500	412	
		341	4570	437	
<b>ADS-C<sub>16</sub>amm</b>	DMF	377	3480	397	0.18
		357	3600	412	
		341	3580	437	
<b>ADS-C<sub>8</sub>benzyl</b>	CH <sub>2</sub> Cl <sub>2</sub>	378	5220	397	0.07
		359	6870	417	
		342	5905	441	
<b>ADS-C<sub>8</sub>benzyl</b>	DMF	377	4452	394	0.17
		358	4801	416	
		341	4405	440	
<b>ADS-C<sub>12</sub>benzyl</b>	CH <sub>2</sub> Cl <sub>2</sub>	378	4550	395	0.06
		358	6005	416	
		341	5040	440	
<b>ADS-C<sub>12</sub>benzyl</b>	DMF	377	3800	394	0.14
		358	5190	416	
		341	4210	440	
<b>ADS-C<sub>16</sub>benzyl</b>	CH <sub>2</sub> Cl <sub>2</sub>	378	3560	392	0.07
		359	4480	412	
		341	4170	438	
<b>ADS-C<sub>16</sub>benzyl</b>	DMF	377	3900	398	0.13
		357	4230	416	
		341	4150	441	

[a] Determined in water, dichloromethane and DMF solutions ( $c \approx 3.10^{-5}$  M) using quinine bisulfate in 1.0N H<sub>2</sub>SO<sub>4</sub> as reference ( $\Phi_{\text{F}}=0.55$  in water,  $\lambda_{\text{exc}}=366$  nm).<sup>[18]</sup> All  $\Phi_{\text{F}}$  values are corrected for changes in refractive index.

on the nature of the counterion. The decrease in the quantum yields in dichloromethane and in DMF is likely due to resonance phenomena involving anthracene and the solvents.<sup>[19]</sup>

**Thermal studies:** The thermal behaviour of the **ADS** ionic complexes was investigated first by polarising optical microscopy (POM) and differential scanning calorimetry (DSC). The transition temperatures and enthalpies are gathered in Table 2. DSC measurements, POM analysis and NMR spectroscopy revealed that the ammonium complexes are stable up to 170–180 °C. Above this temperature, the white pow-

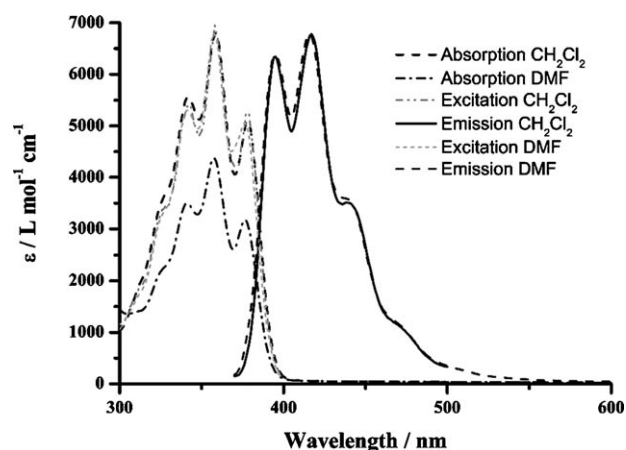


Figure 4. Absorption, emission ( $\lambda_{\text{ex}}=358$  nm) and excitation ( $\lambda_{\text{em}}=416$  nm) spectra of **ADS-C<sub>12</sub>benzyl** in dichloromethane ( $c=3.4 \times 10^{-5}$  mol L<sup>-1</sup>) and DMF ( $c=3.7 \times 10^{-5}$  mol L<sup>-1</sup>).

Table 2. Thermal behaviour of the liquid-crystalline phases.<sup>[a]</sup>

Compound	Transition temperatures [°C]( $\Delta H$ [J g <sup>-1</sup> ])
<b>ADS-DiC<sub>16</sub></b>	Cr 49 (33.8) Cr' 170 (dec)
	Cr' 35 (-33.8) Cr
<b>ADS-DiC<sub>18</sub></b>	Cr 45 (39.5) Cr' 180 (dec)
	Cr' 25 (-40.1) Cr
<b>ADS-C<sub>8</sub>amm</b>	Cr 20 (20.7) Cr' 90 (1.9) Cr'' 180 (dec)
	Cr'' 85 (-1.9) Cr' 12 (-20.7) Cr
	Cr'' 82 (-9.0) Cr' 56 (-40.8) Cr
<b>ADS-C<sub>12</sub>amm</b>	Cr 66 (39.5) Cr' 85 (8.7) Cr'' 180 (dec)
	Cr'' 82 (-9.0) Cr' 56 (-40.8) Cr
	Cr'' 82 (-9.0) Cr' 56 (-40.8) Cr
<b>ADS-C<sub>14</sub>amm</b>	Cr 77 (29.7) Cr' 99 (7.8) Cr'' 170 (dec)
	Cr'' 96 (-7.8) Cr' 66 (-30.8) Cr
	Cr'' 96 (-7.8) Cr' 66 (-30.8) Cr
<b>ADS-C<sub>16</sub>amm</b>	Cr 85 (36.5) Cr' 106 (5.9) Cr'' 170 (dec)
	Cr'' 102 (-7.2) Cr' 69 (-35.7) Cr
	Cr'' 102 (-7.2) Cr' 69 (-35.7) Cr
<b>ADS-C<sub>8</sub>benzyl</b>	Col <sub>h</sub> 73 (-19.1) Cr 129 (27.6) Iso
	Iso 117 (-0.7) Col <sub>h</sub>
	Iso 117 (-0.7) Col <sub>h</sub>
<b>ADS-C<sub>12</sub>benzyl</b>	Col <sub>h</sub> 193 (1.2) Iso
	Iso 189 (-0.9) Col <sub>h</sub>
	Iso 189 (-0.9) Col <sub>h</sub>
<b>ADS-C<sub>16</sub>benzyl</b>	Cr 47 (26.9) Col <sub>h</sub> 240 (dec)
	Col <sub>h</sub> 31 (-28.52) Cr
	Col <sub>h</sub> 31 (-28.52) Cr

[a] Cr, crystalline phase; Iso, isotropic liquid; Col<sub>h</sub>, hexagonal columnar mesophase; dec, decomposition temperature (evaluated from the deviation of the baseline on the DSC curve and confirmed by POM).

ders gradually turn light-brown. The imidazolium salts appear to be more stable and degradation only occurs at temperatures above 240 °C.

**ADS-DiC<sub>n</sub>** ( $n=16, 18$ ): These two complexes display a single reversible transition at 49 °C for **ADS-DiC<sub>16</sub>** and at 45 °C for **ADS-DiC<sub>18</sub>**. POM showed that the compounds are birefringent from room temperature up to the degradation temperature. Thus, the materials are in an organised state from room temperature up to 170 °C. Microscopic observations did not show any clear melting or isotropisation points and, at this stage, the nature of the transitions observed by DSC cannot be precisely assigned.

**ADS-C<sub>n</sub>amm** ( $n=8, 12, 14, 16$ ): All the as-prepared **ADS-C<sub>n</sub>amm** complexes appeared as crystalline powders between

cross-polarisers. Two reversible thermal transitions were observed in the DSC traces for each complex. The transition temperatures increased with the length of the carbon chains. However, POM performed upon heating revealed that the morphology, the birefringence and the stiffness of the crystallites remained intact up to 170–180 °C. The observed transitions can likely be attributed to crystal–crystal transitions (internal reorganisations) and these complexes seem to lack any mesomorphic properties.

**ADS-C<sub>n</sub>benzyl** (*n*=8, 12, 16): The thermal behaviour of **ADS-C<sub>8</sub>benzyl** appears to be more complicated. The first heating curve in the DSC trace shows an endothermic transition centred at 129 °C. POM revealed that above 135 °C the material is in an isotropic fluid state (appears black between crossed-polarisers). Upon cooling (Figure 5a), a small transition was detected at 117 °C and POM performed below this temperature revealed that the material entered into a fluid birefringent mesomorphic state. A texture with small domains readily developed but no clear textural assignment of the symmetry of the mesophase was possible. On a second heating (Figure 5a), an exothermic peak was observed at 73 °C. Such behaviour indicates that the mesophase stabilised after cooling was metastable and the energy imported during the heating stage allowed the compound to melt and to recrystallise in a more stable crystalline phase (Cr). On further heating, an endothermic peak centred at 129 °C was observed and is attributed to the melting of the crystalline phase into the isotropic liquid. Such thermal behaviour is typical of compounds that have a tendency to crystallise but with slow kinetics, probably induced by strong steric constraints. At lower scan rates, enlargement of the signal drastically decreases the intensity of the DSC peaks and no additional information was obtained.

The initial DSC heating curve of the **ADS-C<sub>12</sub>benzyl** complex displays a broad transition centred at 130 °C due to some internal rearrangement. Melting of the compound into an isotropic state was observed on heating to 193 °C (Figure 5b). On cooling the isotropic liquid, the compound became birefringent and a texture typical of a columnar phase with pseudo-fan shapes was observed (Figure 6). The concomitant observation of the soft nature of the material indicates the existence of a mesomorphic state (see below).

The DSC heating curve of the **ADS-C<sub>16</sub>benzyl** complex displays a broad, reversible transition after the first heating cycle centred at 30 °C (Figure 5c). This broad transition is typical of structural rearrangements (melting) of aliphatic chains. Above this transition, the compound became fluid and birefringent, good indicators of mesomorphic nature. The absence of an isotropisation point before the degradation temperature of around 240 °C prevented any definite textural assignment of the phase symmetry.

**XRD characterisation and mesomorphic behaviour:** All the complexes were subjected to a range of temperature-dependent wide- (WAXS) and small-angle (SAXS) X-ray scattering measurements to elucidate their morphologies. All the

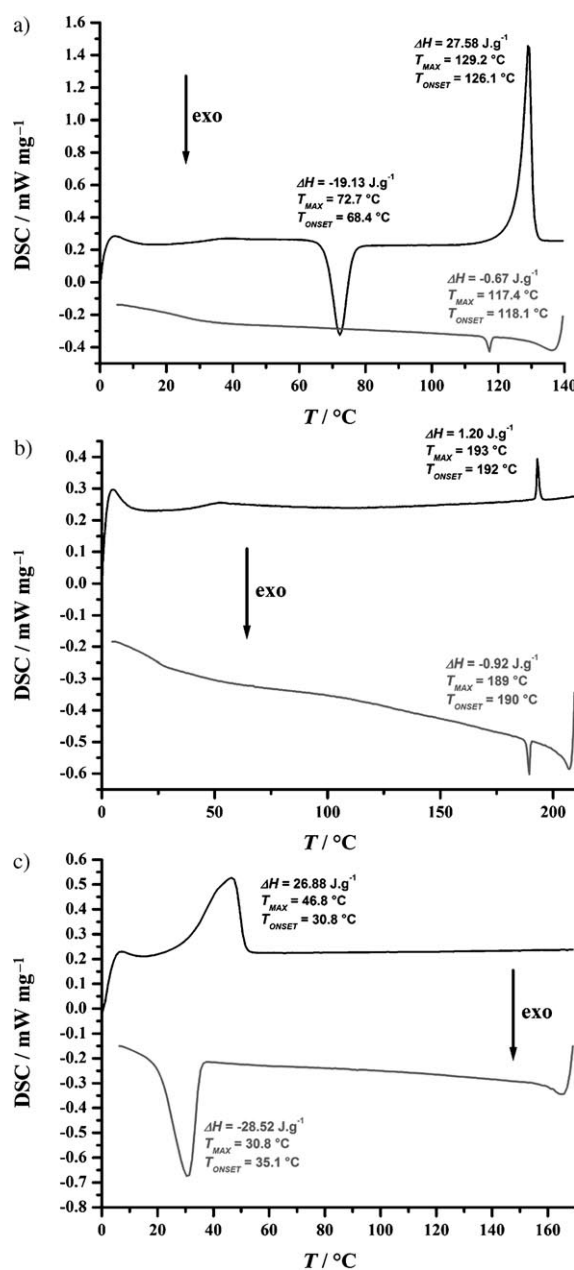


Figure 5. DSC traces of a) **ADS-C<sub>8</sub>benzyl**, b) **ADS-C<sub>12</sub>benzyl** and c) **ADS-C<sub>16</sub>benzyl** showing the second heating curve (black) and the first cooling curve (red).

room-temperature experiments were performed before the high-temperature experiments to minimise any possible effects of thermal degradation. Therefore, for most of the compounds the experiments were performed in the following order: 1) room temperature in the virgin state, 2) room temperature after heating to the temperature appropriate for thermal treatment, in general a temperature above the endothermic transition measured by DSC (temperatures for the thermal treatment: **ADS-DiC<sub>16</sub>**, 120 °C; **ADS-DiC<sub>18</sub>**, 120 °C; **ADS-C<sub>8</sub>amm**, 110 °C; **ADS-C<sub>12</sub>amm**, 78 °C; **ADS-C<sub>14</sub>amm**, 120 °C; **ADS-C<sub>16</sub>amm**, 130 °C; **ADS-C<sub>8</sub>benzyl**, 149 °C; **ADS-C<sub>12</sub>benzyl**, 130 °C; **ADS-C<sub>16</sub>benzyl**, 130 °C) and



Figure 6. The **ADS-C<sub>12</sub>benzyl** compound observed by optical microscopy at 187 °C between crossed-polarisers (symbolised by the cross in the corner of the picture).

3) high-temperature experiment or experiments. The results are gathered in Table 3.

Table 3. X-ray characterisation of the liquid-crystalline phases.<sup>[a]</sup> For each compound the experiments were performed at various temperatures in the order given in the table.

Compound	Temperature [°C]	Phase	<i>hkl</i>	<i>d</i> <sub>meas</sub> [Å]	<i>a</i> [Å]	<i>S</i> [Å <sup>2</sup> ]
<b>ADS-C<sub>8</sub>benzyl</b>	25 <sup>[b]</sup>	Cr				
	25 <sup>[c]</sup>	Col <sub>h</sub>	100	32.2	37.2	1198
	100	Cr	200	16.1		
				4.5 <sup>[d]</sup>		
<b>ADS-C<sub>12</sub>benzyl</b>	25 <sup>[b]</sup>	Cr				
	25 <sup>[c]</sup>	Cr	100	35.1	40.6	1429
	130	Col <sub>h</sub>	200	17.6		
				4.6 <sup>[d]</sup>		
<b>ADS-C<sub>16</sub>benzyl</b>	25 <sup>[b]</sup>	Cr				
	25 <sup>[c]</sup>	Cr	100	38.5	44.5	1713
	130	Col <sub>h</sub>		4.6 <sup>[d]</sup>		

[a] *d*<sub>meas</sub> is the measured diffraction peak spacing; *hkl* is the indexation of the reflections of the Col<sub>h</sub> phase; *a* is the lattice constant of the hexagonal columnar phase; *S* is the lattice area ( $S = a < d_{10} >$  for Col<sub>h</sub>); Cr, crystalline phase; Col<sub>h</sub>, hexagonal columnar mesophase. [b] Virgin sample. [c] After thermal treatment (heating above the thermal transition and cooling to room temperature). [d] Diffuse, broad maximum.

**ADS-DiC<sub>n</sub>** (*n* = 16, 18) and **ADS-C<sub>n</sub>amm** (*n* = 8, 12, 14, 16): The X-ray results indicate that none of these compounds is mesomorphic at the temperatures studied. Instead, all the patterns recorded at room temperature and at high temperatures are characteristic of crystalline phases. Indeed, in all cases the diffraction patterns are complex and contain a high number of sharp maxima in the whole angular range, which is typical of well-organised crystalline complexes.

**ADS-C<sub>n</sub>benzyl** (*n* = 8, 12, 16): At high temperatures these compounds gave X-ray patterns characteristic of a liquid crystal phase (Table 3). This was deduced from the presence of one or two sharp reflections in the low-angle region and the absence of maxima in the high-angle region, except for a broad, diffuse halo, typically observed in all kinds of meso-

phases and characteristic of the liquid-like order of the hydrocarbon chains (Figure 7).

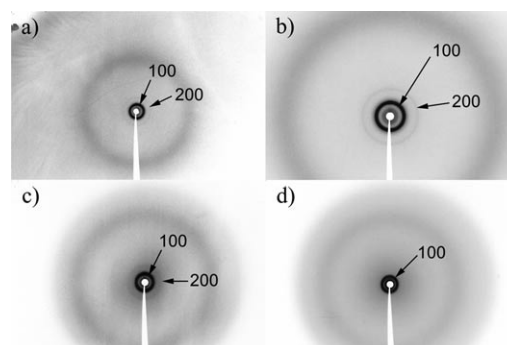


Figure 7. XRD patterns of a) **ADS-C<sub>8</sub>benzyl** in the hexagonal columnar phase at room temperature after heating at 110 °C, b) the same compound under the same conditions in the small-angle region, c) **ADS-C<sub>12</sub>benzyl** in the hexagonal columnar phase at 130 °C, and d) **ADS-C<sub>16</sub>benzyl** in the hexagonal columnar phase at 130 °C.

As mentioned earlier, the behaviour of the **ADS-C<sub>8</sub>benzyl** complex is peculiar for two reasons: 1) the mesophase froze at room temperature, at least for some time (the time of the exposure to X rays) and 2) when the frozen mesophase was heated up to 100 °C it crystallised. The X-ray results confirm that the mesophase stabilised after cooling was metastable and that heating allowed the compound to recrystallise in a more stable crystalline phase (Cr).

Concerning the type of mesophase found in these compounds, the set of one or two reflections found in the low-angle region has two possible interpretations. 1) The diffraction peak(s) could be the first (and second)-order reflection(s) of a layer structure (smectic mesophase). In that case the spacing of the first reflection (or the double of the second reflection) is the layer thickness. 2) The peak(s) is (are) the (100) (and (200)) reflection(s) from a hexagonal columnar mesophase, the (110) reflection being absent.<sup>[20]</sup>

The second interpretation is the most reasonable. This conclusion is based on the following arguments. 1) The molecular structure of the **C<sub>n</sub>benzyl<sup>+</sup>** cation contains three long chains attached to the aromatic unit and the spatial requirements of these chains are impossible to fulfil in a smectic structure owing to the mismatch between the cross-section of the aromatic moiety and the total cross-section of the hydrocarbon chains.<sup>[21]</sup> Instead, the chains have more space available in a columnar structure in which they spread out around the central core of the column. 2) If the mesophase was smectic, very simple calculations would allow the molecular cross-section to be estimated. If the density is known, the molecular volume can be deduced from the molecular mass ( $V_m = M/0.6022\rho$ , with  $V_m$  the molecular volume in Å<sup>3</sup>,  $M$  the molecular mass and  $\rho$  the density in g cm<sup>-3</sup>). Dividing the molecular volume by the layer thickness (*d*) gives the cross-section of a molecule in the plane of the smectic layer. The calculated molecular cross-sections are  $75/\rho$  Å<sup>2</sup> for **ADS-C<sub>8</sub>benzyl**,  $84/\rho$  Å<sup>2</sup> for **ADS-C<sub>12</sub>benzyl** and  $92/\rho$  Å<sup>2</sup> for

**ADS-C<sub>16</sub>benzyl.** Because the density must be similar for the three compounds (in fact, it is usually assumed that density is close to 1 g cm<sup>-3</sup> for organic compounds), this would mean that the cross-section increases upon increasing the number of carbon atoms in the chains (18% from  $n=8$  to  $n=16$ ). This is not consistent with a smectic structure because lengthening of the hydrocarbon chains should increase the length of the molecule but not its thickness. On the other hand, if the mesophase is columnar hexagonal and we deduce the molecular volume  $V_m$  by using the above equation, then the height of column  $h$  occupied by each molecule can be estimated to be  $h = V_m/S$ , with  $S$  the area of the two-dimensional hexagonal cell ( $S = ad_{\text{meas}}$ ). The results of these calculations are  $h = 2.02/\rho \text{ \AA}$  for **ADS-C<sub>8</sub>benzyl** at room temperature,  $h = 2.08/\rho \text{ \AA}$  for **ADS-C<sub>12</sub>benzyl** and  $h = 2.06/\rho \text{ \AA}$  for **ADS-C<sub>16</sub>benzyl**. The variation is 3%, that is, the estimated values for  $h$  are practically the same for the three compounds. This is consistent with the mesophase being columnar, because for this kind of mesophase lengthening the hydrocarbon chains is expected to increase only the diameter of the column but not the stacking distance. It is evident that one single molecule cannot be located in a "slice" of about 2–2.1 Å thickness, but it is reasonable that two molecules are contained in a "slice" of 4–4.2 Å, assuming a density of 1 g cm<sup>-3</sup> (4.5–4.6 Å if the density is 0.9 g cm<sup>-3</sup>). The  $S$  values for the three compounds are, respectively, 1198 (at RT), 1429 (at 130°C), and 1713 Å<sup>2</sup> (at 130°C). These values follow a logical evolution as they are proportional to the molecular masses.

Note that for **ADS-C<sub>12</sub>benzyl**, a crystallisation process was observed by XRD at room temperature after the thermal treatment whereas no peak associated with such a mesophase-to-crystal transition was detected by DSC. DSC and XRD analysis imply different heating and cooling rates and this behaviour can be explained by a tendency of the product to slowly crystallise at low temperatures during the XRD measurements.

**Packing study of the ISA complexes in their liquid-crystalline phases:** To gain some insight into the packing of the **ADS-C<sub>n</sub>benzyl** complexes inside the columnar liquid-crystalline phases, a standard geometrical treatment was applied.<sup>[22]</sup> As already mentioned, columnar packing is characterised by the columnar cross-section  $S_{\text{col}}$  and the stacking periodicity  $h$  along the columnar axis, both parameters being analytically linked through the relation  $hS_{\text{col}} = ZV_m$ , with  $Z$  the number of molecules within a columnar stratum (disc)  $h$  thick and  $V_m$  the molecular volume. In the XRD patterns, neither a peak nor a halo related to the stacking periodicity  $h$  was observed. In this situation, it is difficult to determine the number of molecules per disc and only rough estimations can be made. It was found (see above) that two molecules are contained in a "slice" of 4–4.2 Å, assuming a density of 1 g cm<sup>-3</sup> (4.5–4.6 Å if the density is 0.9 g cm<sup>-3</sup>). This implies that each disc, generating columns by stacking, is formed by two complexes (Figure 8).<sup>[14]</sup> The ionic groups are located in the centre of the disc and the peripheral chains surround the

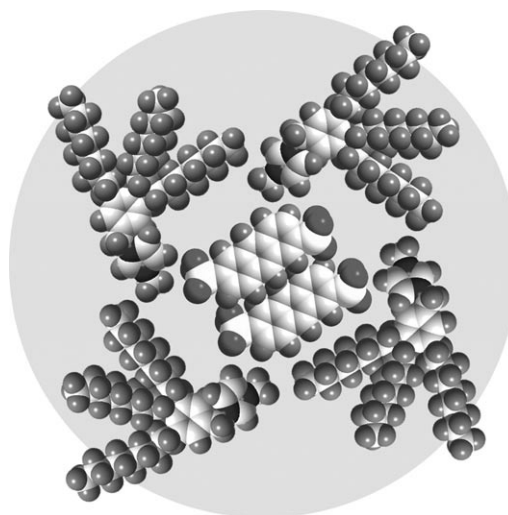


Figure 8. Suggested molecular organisation based on the X-ray data for **ADS-C<sub>n</sub>benzyl** complexes inside the hexagonal columnar phase.

central ionic region. In this way, optimal microsegregation between the aliphatic and polar parts inside a disc is ensured. The hydrocarbon chains are able to efficiently fill the peripheral space around the columnar core. The mutual organisation of these columns into a hexagonal lattice leads to the formation of the mesophase. However, this is a simplified model because, in fact, the molecules can aggregate in such a way that the cations are randomly oriented, with just their tips pointing towards the stacked anion column without the need to form discrete discs.

**Solid-state luminescence:** The emission properties in the solid state were also evaluated directly by using isolated powders and a spectrophotometer equipped with an optical fibre. The emission spectrum of the starting compound **ADS-K** shows a broad emission band, weakly structured, centred at 437 nm (Figure 9). The redshifts observed in the emission spectra compared to the emission in fluid solution, are attributed to the head-to-tail orientation or the  $J$  aggregates of the **ADS<sup>2-</sup>** ions in the solid state.<sup>[23]</sup> A redshift of the absorption spectrum, associated with the formation of head-to-tail anthracene aggregates, should also be observed.<sup>[24]</sup> The photoluminescence spectra of all the as-prepared **ADS-C<sub>n</sub>amm** and **ADS-DiC<sub>n</sub>** complexes present well-structured emission bands with maxima located at 410, 435 and 460 nm at room temperature. The positions of the emission bands of these crystalline materials (cf. Table 1) are comparable to those observed for the **ADS<sup>2-</sup>** ion isolated in DMF or in dichloromethane. The introduction of long carbon chains into the ammonium counterions results in the isolation of the anthracene residues in crystalline solids, as seen in the crystal structure of the **ADS-DiC<sub>16</sub>** complex (see above).

For all the **ADS-C<sub>n</sub>benzyl** complexes, a slight redshift of the emission bands was observed, which indicates that the trialkoxybenzylimidazolium fragments do not prevent the

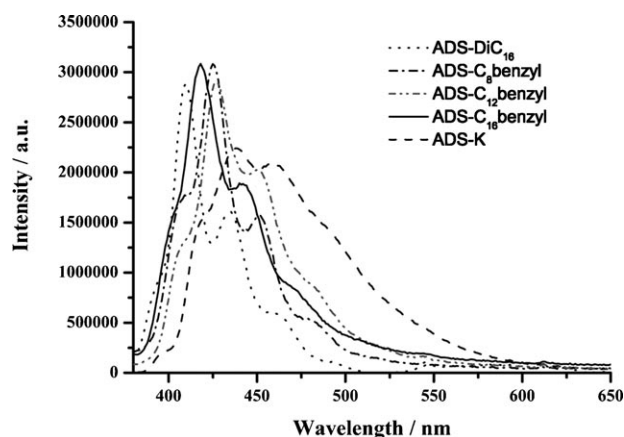


Figure 9. Solid-state emission spectra of the as-prepared **ADS-K**, **ADS-DiC16**, **ADS-C<sub>8</sub>benzyl**, **ADS-C<sub>12</sub>benzyl** and **ADS-C<sub>16</sub>benzyl** complexes at room temperature under excitation at 360 nm.

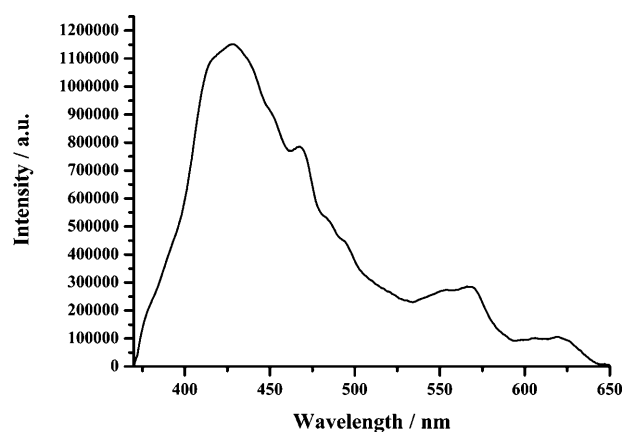


Figure 10. Fluorescence spectra of **ADS-C<sub>16</sub>benzyl** at 100°C in the hexagonal columnar mesophase.

formation of aggregated anthracene species. The fact that the redshift observed with the **ADS-K** complex (28 nm) was larger than those observed with the **ADS-C<sub>n</sub>benzyl** complexes suggests that the distance between the anthracene molecules with potassium counterions is shorter and thus that stronger intermolecular interactions occur in the solid state, which leads to higher-order aggregates. In the series of **ADS-C<sub>n</sub>benzyl** complexes, the redshift decreases with the chain lengths (17 nm for  $n=8$ , 12 nm for  $n=12$ , 5 nm for  $n=16$ ) and this can be attributed to a decrease in the intermolecular interactions between the anthracene moieties as the trialkoxybenzyl template becomes bulkier. The emission band of the **ADS-C<sub>8</sub>benzyl** complex was more extended, even below 420 nm, an observation in keeping with stronger intermolecular interactions in the solid state.

Temperature-dependent fluorescence measurements were also performed on the liquid crystalline **ADS-C<sub>n</sub>benzyl** ( $n=8, 12, 16$ ) compounds by using a heating stage. The luminescence spectrum of **ADS-C<sub>16</sub>benzyl** measured at 100°C in its columnar mesophase displays a broad, structureless emission band centred around 431 nm (Figure 10). This redshifted broad emission band indicates that intermolecular interactions between the anthracene moieties take place in the mesophase and this is in line with the formation of a columnar core containing mainly anthracene fragments (see model). Upon cooling at 10°C min<sup>-1</sup>, no real changes were observed in the fluorescence spectra, in line with the DSC measurements. The extension of luminescence up to 650 nm in the mesophases is also indicative of the formation of higher-order aggregates in the liquid-crystalline state.

The mesomorphic complexes were also examined by fluorescence microscopy on a heating stage. Upon cooling, the materials became liquid-crystalline, enabling the formation of homogeneous thin films. The fluid materials showed a homogeneous blue luminescence, which is typical of anthracene moieties (Figure 11). Note that the complexes were still luminescent at elevated temperatures. Despite the formation of well-defined textures with **ADS-C<sub>12</sub>benzyl**, no do-

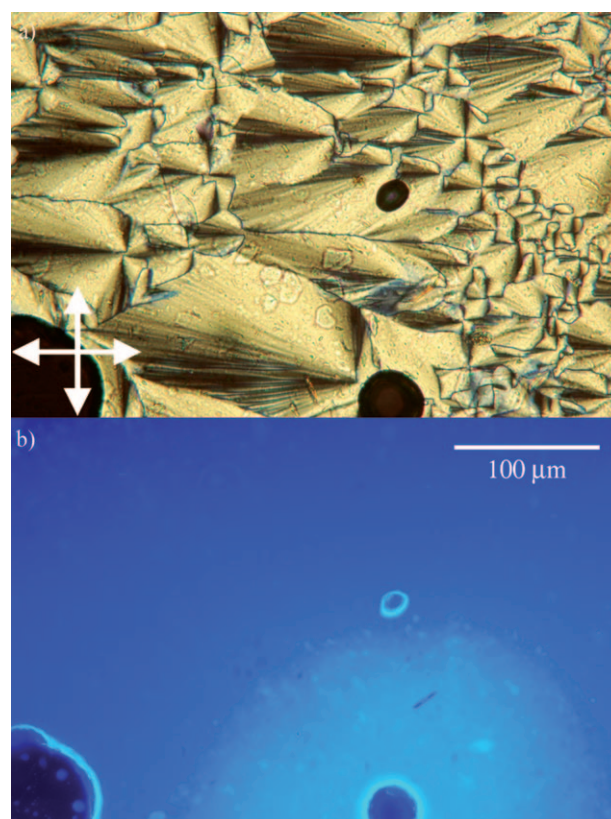


Figure 11. A drop of **ADS-C<sub>12</sub>benzyl** observed by optical microscopy at 187°C a) with a white light in transmission between crossed-polarisers (symbolised by the cross in the corner of the picture; classical texture) and b) upon irradiation at  $300 < \lambda_{ex} < 350$  nm.

mains with different emissions have been observed at this stage.<sup>[14,25]</sup>

## Conclusions

A series of functional salts have been synthesised by ionic self-assembly from a charged luminescent anthracene core

and various types of non-luminescent amphiphilic ammonium and imidazolium cations. The crystal structure of the **ADS-DiC<sub>16</sub>** complex revealed that the long carbon chains can be fully intercalated between the anthracene moieties and that microsegregation between anions and cations will be more difficult to induce with polyaromatic fragments and long carbon chains. The affinity between the long carbon chains and the anthracene core clearly prevents the formation of mesomorphic materials and stable crystal structures were isolated. Solid-state fluorescence measurements performed on these crystalline structures displayed emission properties identical to those of the isolated molecules in solution. The measurements confirm that the anthracene core has a strong tendency to form crystalline structures with ammonium cations carrying long carbon chains and that the aliphatic parts efficiently segregate the anthracene moieties. The use of imidazolium in place of the ammonium cations has allowed the formation of mesomorphic materials with the negatively charged **ADS<sup>2-</sup>** core through an ionic self-assembly process. The use of imidazolium-grafted-trialkoxybenzyl salts allowed the formation of columnar mesophases with hexagonal symmetry, unambiguously identified by X-ray scattering measurements at various temperatures and by the typical textures observed between crossed-polarisers by optical microscopy. From these data it is estimated that for the **ADS-C<sub>n</sub>benzyl** complexes, two associated pairs form discs able to pile up to form the column. The use of a highly luminescent platform allowed the homogeneity and quality of the thin films to be checked by fluorescence microscopy. Solid-state fluorescence measurements showed that the anthracene anions were not fully isolated and that *J* aggregates formed inside the mesophases. The use of ionic self-assembled complexes provides a relatively easy way to produce liquid-crystalline materials and thin films stable over a large temperature range that are possibly useful for applications in electrical devices. Work along these lines is in progress.

## Experimental Section

The 300 (<sup>1</sup>H), 400 (<sup>1</sup>H) and 75.5 MHz (<sup>13</sup>C) NMR spectra were recorded at room temperature using perdeuterated solvents as internal standards. A ZAB-HF-VB-analytical apparatus in FAB<sup>+</sup> mode was used with *m*-nitrobenzyl alcohol (*m*-NBA) as a matrix. Chromatographic purification was conducted using 40–63 μm silica gel. Thin-layer chromatography (TLC) was performed on silica gel plates coated with fluorescent indicator. FTIR spectra were recorded by using a Perkin–Elmer “spectrum one” spectrometer equipped with an ATR diamond apparatus. UV/Vis spectra were recorded by using a Shimadzu UV-3600 dual-beam grating spectrophotometer with a 1 cm quartz cell. Fluorescence spectra were recorded on a HORIBA Jobin–Yvon Fluoromax 4P spectrofluorimeter with a 1 cm quartz cell for solutions or an optical fibre for solids. Temperature-dependent luminescence measurements were performed on thin films by using the HORIBA Jobin–Yvon Fluoromax 4P spectrofluorimeter equipped with an optical fibre and a heating stage (Linkam LTS350 hot stage and a Linkam TMS94 central processor). All fluorescence spectra were corrected. The fluorescence quantum yields ( $\phi_{\text{exp}}$ ) were calculated from Equation (1) in which *F* denotes the integral of the corrected fluorescence spectrum, *A* is the absorbance at the excitation wavelength

and *n* is the refractive index of the medium. The reference system used was rhodamine 6G in methanol ( $\phi_{\text{ref}}=0.78$ ,  $\lambda_{\text{exc}}=488$  nm).

$$\Phi_{\text{exp}} = \Phi_{\text{ref}} \frac{F[1 - \exp(-A_{\text{ref}} \ln 10)]n^2}{F_{\text{ref}}[1 - \exp(-A \ln 10)]n_{\text{ref}}^2} \quad (1)$$

Differential scanning calorimetry (DSC) was performed on a Netzsch DSC 200 PC/1M/H Phox instrument equipped with an intracooler, allowing measurements from –65 °C up to 450 °C. The samples were examined at a scan rate of 10 K min<sup>-1</sup> by applying two heating and one cooling cycles. The apparatus was calibrated with indium (156.6 °C). The phase behaviour was studied by polarising optical microscopy (POM) on a Leica DMLB microscope equipped with a Linkam LTS350 hot-stage and a Linkam TMS94 central processor. The XRD patterns were obtained with a pinhole camera (Anton-Paar) operating with a point-focussed Ni-filtered Cu<sub>Kα</sub> beam. The samples were held in Lindemann glass capillaries (0.9 mm diameter) and heated, when necessary, with a variable-temperature oven. The patterns were collected on flat photographic film perpendicular to the X-ray beam. Spacings were obtained by application of Bragg’s law.

**General procedure for the synthesis of the [ADS-DiC<sub>n</sub>] complexes (n = 16, 18):** The sulfonate salt (50 mg, 0.12 mmol) and 2 equiv of the **DiC<sub>n</sub>** salts (0.24 mmol) were stirred overnight in DMF (25 mL) at 70 °C. After cooling to room temperature, water was added to precipitate the complex. The complex was washed with water (3 × 15 mL). After drying, the precipitate was dissolved in CH<sub>2</sub>Cl<sub>2</sub> and filtered through Celite to remove any insoluble material. The complex was recrystallised from a CH<sub>2</sub>Cl<sub>2</sub>/CH<sub>3</sub>CN mixture by slow evaporation of the dichloromethane.

**ADS-DiC<sub>16</sub>:** Isolated yield: 25%. <sup>1</sup>H NMR ([D<sub>6</sub>]DMSO, 300 MHz):  $\delta$  = 0.85 (t, <sup>3</sup>*J* = 6.7 Hz, 12H), 1.24 (brs, 104H), 1.615 (brs, 8H), 2.97 (s, 12H, NCH<sub>3</sub>), 3.20 (m, 8H, NCH<sub>2</sub>), 7.68 (dd, <sup>3</sup>*J* = 8.8, <sup>4</sup>*J* = 1.6 Hz, 2H), 8.01 (d, <sup>3</sup>*J* = 8.8 Hz, 2H), 8.27 (s, 2H), 8.59 ppm (s, 2H); IR (ATR):  $\tilde{\nu}$  = 2918 (vs) ( $\nu_{\text{as}}\text{CH}_2$ ), 2850 (vs) ( $\nu_{\text{s}}\text{CH}_2$ ), 1495 (m), 1468 (s), 1397 (w), 1375 (w), 1342 (w), 1292 (w), 1276 (m), 1261 (m), 1236 (s), 1215 (vs), 1203 (vs), 1178 (vs), 1152 (m), 1130 (w), 1089 (m), 1079 (vs), 1022 (vs), 958 (w), 926 (w), 908 (s), 900 (m), 869 (w), 860 (w), 831 cm<sup>-1</sup> (w); elemental analysis calcd (%) for C<sub>82</sub>H<sub>152</sub>N<sub>2</sub>O<sub>6</sub>S<sub>2</sub>: C 74.26, H 11.55, N 2.11; found: C 74.84, H 11.71, N 1.89.

**ADS-DiC<sub>18</sub>:** Isolated yield: 41%. <sup>1</sup>H NMR ([D<sub>6</sub>]DMSO, 400 MHz, 70 °C):  $\delta$  = 0.87 (t, <sup>3</sup>*J* = 5.1 Hz, 12H), 1.27 (brs, 120H), 1.66 (brs, 8H), 2.99 (s, 12H, NCH<sub>3</sub>), 3.23 (m, 8H, NCH<sub>2</sub>), 7.73 (d, <sup>3</sup>*J* = 9.0 Hz, 2H), 7.99 (d, <sup>3</sup>*J* = 8.6 Hz, 2H), 8.29 (s, 2H), 8.53 ppm (s, 2H); IR (ATR):  $\tilde{\nu}$  = 2917 (vs) ( $\nu_{\text{as}}\text{CH}_2$ ), 2850 (vs) ( $\nu_{\text{s}}\text{CH}_2$ ), 1496 (m), 1468 (s), 1396 (w), 1378 (w), 1342 (w), 1292 (w), 1273 (w), 1261 (m), 1235 (s), 1216 (vs), 1202 (vs), 1178 (vs), 1152 (m), 1130 (w), 1089 (m), 1079 (vs), 1022 (vs), 987 (w), 949 (w), 926 (m), 908 (s), 900 (m), 869 (w), 860 (w), 831 cm<sup>-1</sup> (w); elemental analysis calcd (%) for C<sub>90</sub>H<sub>168</sub>N<sub>2</sub>O<sub>6</sub>S<sub>2</sub>: C 75.15, H 11.77, N 1.95; found: C 75.44, H 11.52, N 1.70.

**General procedure for the synthesis of the [ADS-C<sub>n</sub>amm] complexes (n = 8, 12, 14, 16):** The sulfonate salt (1 equiv) was dissolved in DMF (2 mg mL<sup>-1</sup>) and **C<sub>n</sub>amm** (1 equiv per negative charge) was added. The mixture was stirred at 60 °C for one night. After cooling, water was then added and the precipitate washed with water and dried under vacuum. Crystallisation from a CH<sub>2</sub>Cl<sub>2</sub>/CH<sub>3</sub>CN mixture gave the complexes as powders.

**ADS-C<sub>8</sub>amm:** Isolated yield: 30%. <sup>1</sup>H NMR (DMSO, 300 MHz):  $\delta$  = 0.86 (m, 18H), 1.16–1.53 (m, 60H), 1.58–1.82 (m, 12H), 3.59 (s, 18H), 3.93 (t, <sup>3</sup>*J* = 6.2 Hz, 4H), 4.04 (t, <sup>3</sup>*J* = 6.1 Hz, 8H), 7.25 (s, 4H), 7.68 (dd, <sup>3</sup>*J* = 8.8, <sup>4</sup>*J* = 1.3 Hz, 2H), 7.95 (s, 8H), 8.01 (d, <sup>3</sup>*J* = 8.7 Hz, 2H), 8.27 (s, 2H), 8.59 (s, 2H), 10.36 ppm (s, NH, 2H); IR (ATR):  $\tilde{\nu}$  = 3314 (br w) ( $\nu_{\text{NH}}$ ), 2922 (s) ( $\nu_{\text{as}}\text{CH}_2$ ), 2854 (s) ( $\nu_{\text{s}}\text{CH}_2$ ), 1666 (s) ( $\nu_{\text{CO}}$ ), 1606 (m), 1583 (s), 1542 (s), 1513 (m), 1498 (s), 1468 (s), 1427 (s), 1410 (m), 1378 (w), 1331 (vs), 1294 (w), 1275 (w), 1259 (w), 1219 (vs), 1182 (vs), 1110 (vs), 1082 (vs), 1023 (vs), 986 (w), 960 (w), 936 (w), 911 (m), 874 (w), 846 (m), 812 cm<sup>-1</sup> (w); elemental analysis calcd (%) for C<sub>94</sub>H<sub>142</sub>N<sub>4</sub>O<sub>4</sub>S<sub>2</sub>: C 69.85, H 8.86, N 3.47; found: C 70.12, H 9.17, N 3.22.

**ADS-C<sub>12</sub>amm:** Isolated yield: 47%. <sup>1</sup>H NMR (DMSO, 300 MHz):  $\delta$  = 0.85 (m, 18H), 1.08–1.55 (m, 108H), 1.57–1.84 (m, 12H), 3.59 (s, 18H),

3.92 (m, 4H), 4.04 (m, 8H), 7.24 (s, 4H), 7.68 (d,  $^3J=7.9$  Hz, 2H), 7.95 (s, 8H), 8.02 (d,  $^3J=8.8$  Hz, 2H), 8.27 (s, 2H), 8.60 (s, 2H), 10.35 ppm (s, NH, 2H); IR (ATR):  $\tilde{\nu}=3301$  (br w) (vNH), 2918 (s) (v<sub>as</sub>CH<sub>2</sub>), 2850 (s) (v<sub>s</sub>CH<sub>2</sub>), 1665 (s) (vCO), 1609 (m), 1581 (s), 1545 (s), 1517 (m), 1499 (s), 1473 (s), 1427 (m), 1409 (w), 1388 (w), 1333 (vs), 1294 (w), 1277 (w), 1253 (w), 1222 (vs), 1196 (m), 1183 (vs), 1158 (m), 1129 (w), 1105 (vs), 1083 (vs), 1026 (vs), 994 (w), 972 (w), 940 (w), 929 (w), 910 (m), 869 (w), 845 (m), 813 cm<sup>-1</sup> (w); elemental analysis calcd (%) for C<sub>118</sub>H<sub>190</sub>N<sub>4</sub>O<sub>14</sub>S<sub>2</sub>: C 72.57, H 9.81, N 2.87; found: C 72.64, H 10.44, N 3.22.

**ADS-C<sub>14</sub>amm:** Isolated yield: 39%. <sup>1</sup>H NMR (DMSO, 400 MHz, 70 °C):  $\delta=0.87$  (t,  $^3J=6.5$  Hz, 18H), 1.20–1.55 (m, 132H), 1.64–1.83 (m, 12H), 3.62 (s, 18H), 3.99 (t,  $^3J=6.5$  Hz, 4H), 4.07 (t,  $^3J=6.3$  Hz, 8H), 7.27 (s, 4H), 7.73 (d,  $^3J=9.4$  Hz, 2H), 7.87–8.03 (m, 10H), 8.29 (s, 2H), 8.52 (s, 2H), 10.12 ppm (s, NH, 2H); IR (ATR):  $\tilde{\nu}=3314$  (br w) (vNH), 2917 (vs) (v<sub>as</sub>CH<sub>2</sub>), 2850 (vs) (v<sub>s</sub>CH<sub>2</sub>), 1665 (s) (vCO), 1609 (m), 1582 (s), 1546 (s), 1516 (m), 1500 (vs), 1473 (s), 1466 (s), 1427 (m), 1388 (w), 1335 (vs), 1294 (w), 1276 (w), 1259 (w), 1223 (vs), 1196 (m), 1184 (vs), 1158 (m), 1129 (w), 1105 (vs), 1083 (vs), 1027 (vs), 997 (w), 973 (w), 939 (w), 929 (w), 910 (m), 869 (w), 841 (m), 814 cm<sup>-1</sup> (w); elemental analysis calcd (%) for C<sub>130</sub>H<sub>214</sub>N<sub>4</sub>O<sub>14</sub>S<sub>2</sub>: C 73.61, H 10.17, N 2.64; found: C 73.95, H 10.49, N 2.99.

**ADS-C<sub>16</sub>amm:** Isolated yield: 40%. <sup>1</sup>H NMR (DMSO, 400 MHz, 80 °C):  $\delta=0.87$  (m, 18H), 1.18–1.56 (m, 156H), 1.65–1.83 (m, 12H), 3.62 (s, 18H), 3.99 (t,  $^3J=6.3$  Hz, 4H), 4.07 (t,  $^3J=6.0$  Hz, 8H), 7.27 (s, 4H), 7.73 (d,  $^3J=9.0$  Hz, 2H), 7.86–8.02 (m, 10H), 8.29 (s, 2H), 8.51 (s, 2H), 10.11 ppm (s, NH, 2H); IR (ATR):  $\tilde{\nu}=3311$  (br w) (vNH), 2917 (vs) (v<sub>as</sub>CH<sub>2</sub>), 2850 (vs) (v<sub>s</sub>CH<sub>2</sub>), 1665 (s) (vCO), 1609 (m), 1582 (s), 1546 (s), 1516 (m), 1500 (vs), 1473 (s), 1466 (s), 1427 (m), 1388 (w), 1335 (vs), 1292 (w), 1277 (w), 1252 (w), 1223 (vs), 1184 (vs), 1158 (w), 1129 (w), 1106 (vs), 1084 (vs), 1027 (vs), 1015 (m), 990 (w), 969 (w), 940 (w), 910 (m), 869 (w), 847 (m), 812 cm<sup>-1</sup> (w); elemental analysis calcd (%) for C<sub>142</sub>H<sub>238</sub>N<sub>4</sub>O<sub>14</sub>S<sub>2</sub>: C 74.49, H 10.48, N 2.45; found: C 74.82, H 10.88, N 2.22.

**General procedure for the synthesis of the [ADS-C<sub>n</sub>benzyl] complexes (n = 8, 12, 16):** The sulfonate salt (1 equiv) was dissolved in DMF (2 mg mL<sup>-1</sup>) and the C<sub>n</sub>benzyl (1 equiv per negative charge) was added. The mixture was stirred at 60 °C for one night. After cooling, water was added and the precipitate was washed with water and dried under vacuum. **ADS-C<sub>12</sub>benzyl** and **ADS-C<sub>16</sub>benzyl** were recrystallised in hot DMSO and **ADS-C<sub>8</sub>benzyl** was recrystallised in a CH<sub>2</sub>Cl<sub>2</sub>/AcOEt mixture by slow evaporation of dichloromethane.

**ADS-C<sub>8</sub>benzyl:** Isolated yield: 45%. <sup>1</sup>H NMR (DMSO, 300 MHz):  $\delta=0.82$ –0.86 (m, 18H), 1.24–1.42 (m, 60H), 1.55–1.73 (m, 12H), 3.78–3.83 (m, 10H), 3.92 (t,  $^3J=6.0$  Hz, 8H), 5.24 (s, 4H), 6.78 (s, 4H), 7.66–7.69 (m, 4H), 7.80 (s, 2H), 8.01 (d,  $^3J=8.7$  Hz, 2H), 8.27 (s, 2H), 8.59 (s, 2H), 9.15 ppm (s, 2H); IR (ATR):  $\tilde{\nu}=2952$  (w) (v<sub>as</sub>CH<sub>3</sub>), 2924 (vs) (v<sub>as</sub>CH<sub>2</sub>), 2867 (w) (v<sub>s</sub>CH<sub>3</sub>), 2852 (vs) (v<sub>s</sub>CH<sub>2</sub>), 1588 (m), 1564 (w), 1504 (m), 1469 (m), 1453 (m), 1442 (m), 1382 (w), 1363 (w), 1334 (m), 1224 (s), 1189 (s), 1113 (s), 1086 (s), 1023 (s), 965 (w), 952 (m), 930 (w), 907 (m), 873 (w), 833 (w), 816 cm<sup>-1</sup> (w); elemental analysis calcd (%) for C<sub>84</sub>H<sub>130</sub>N<sub>4</sub>O<sub>12</sub>S<sub>2</sub>: C 69.48, H 9.02, N 3.86; found: C 69.64, H 9.02, N 3.86.

**ADS-C<sub>12</sub>benzyl:** Isolated yield: 70%. <sup>1</sup>H NMR (DMSO, 200 MHz):  $\delta=0.80$ –0.86 (m, 18H), 1.12–1.71 (m, 120H), 3.76–3.83 (m, 10H), 3.92 (t,  $^3J=6.4$  Hz, 8H), 5.23 (s, 4H), 6.77 (s, 4H), 7.66–7.69 (m, 4H), 7.80 (s, 2H), 8.01 (d,  $^3J=8.8$  Hz, 2H), 8.26 (s, 2H), 8.60 (s, 2H), 9.14 ppm (s, 2H); IR (ATR):  $\tilde{\nu}=2957$  (w) (v<sub>as</sub>CH<sub>3</sub>), 2919 (vs) (v<sub>as</sub>CH<sub>2</sub>), 2864 (w) (v<sub>s</sub>CH<sub>3</sub>), 2850 (vs) (v<sub>s</sub>CH<sub>2</sub>), 1587 (m), 1562 (w), 1504 (m), 1465 (m), 1453 (m), 1441 (m), 1384 (w), 1363 (w), 1335 (m), 1223 (s), 1190 (s), 1115 (s), 1086 (s), 1023 (s), 965 (w), 952 (m), 930 (w), 907 (m), 873 (w), 833 (w), 816 cm<sup>-1</sup> (w); elemental analysis calcd (%) for C<sub>107</sub>H<sub>178</sub>N<sub>4</sub>O<sub>12</sub>S<sub>2</sub>: C 72.52, H 10.03, N 3.13; found: C 72.84, H 10.37, N 3.52.

**ADS-C<sub>16</sub>benzyl:** Isolated yield: 65%. <sup>1</sup>H NMR (DMSO, 300 MHz, 60 °C):  $\delta=0.84$ –0.87 (m, 18H), 1.25–1.47 (m, 156H), 1.60–1.74 (m, 12H), 3.83–3.87 (m, 10H), 3.95 (t,  $^3J=6.4$  Hz, 8H), 5.25 (s, 4H), 6.74 (s, 4H), 7.65–7.66 (m, 2H), 7.71 (d,  $^3J=8.4$  Hz, 2H), 7.73–7.75 (m, 2H), 7.99 (d,  $^3J=8.8$  Hz, 2H), 8.28 (s, 2H), 8.54 (s, 2H), 9.10 ppm (s, 2H); IR (ATR):  $\tilde{\nu}=2957$  (w) (v<sub>as</sub>CH<sub>3</sub>), 2915 (vs) (v<sub>as</sub>CH<sub>2</sub>), 2862 (w) (v<sub>s</sub>CH<sub>3</sub>), 2850 (vs) (v<sub>s</sub>CH<sub>2</sub>), 1587 (m), 1504 (m), 1469 (m), 1456 (m), 1441 (m), 1382 (w),

1364 (w), 1334 (m), 1223 (s), 1183 (s), 1113 (s), 1095 (s), 1085 (s), 1024 (s), 992 (m), 968 (w), 922 (m), 873 (w), 837 (w), 817 cm<sup>-1</sup> (w); elemental analysis calcd (%) for C<sub>132</sub>H<sub>226</sub>N<sub>4</sub>O<sub>12</sub>S<sub>2</sub>: C 74.60, H 10.72, N 2.64; found: C 74.92, H 11.05, N 3.09.

CCDC-720448 contains the supplementary crystallographic data for this paper. These data can be obtained free of charge from The Cambridge Crystallographic Data Centre via [www.ccdc.cam.ac.uk/data\\_request/cif](http://www.ccdc.cam.ac.uk/data_request/cif)

## Acknowledgements

This work was jointly supported by the University of Strasbourg through the European School of Polymer and Materials Chemistry (ECPM) and by the Centre National de la Recherche Scientifique (CNRS) of France. Financial support from the MICINN-FEDER Spanish project CTQ2006-15611-C02-01 is gratefully acknowledged. We are indebted to Professor J. Harrowfield from ISIS in Strasbourg, for his comments on the manuscript prior to publication.

- a) M. O'Neill, S. M. Kelly, *Adv. Mater.* **2003**, *15*, 1135–1146; b) T. Kato, *Science* **2002**, *295*, 2414–2418; c) T. Kato, N. Mizoshita, K. Kishimoto, *Angew. Chem.* **2006**, *118*, 44–74; *Angew. Chem. Int. Ed.* **2006**, *45*, 38–68.
- S. Laschat, A. Baro, N. Steinke, F. Giesselmann, C. Hägele, G. Scalia, R. Judele, E. Kapatsina, S. Sauer, A. Schreivogel, M. Tosoni, *Angew. Chem.* **2007**, *119*, 4916–4973; *Angew. Chem. Int. Ed.* **2007**, *46*, 4832–4887.
- a) D. Adam, P. Schuhmacher, J. Simmerer, L. Häussling, K. Siemsmeyer, K. H. Etzbach, H. Ringsdorf, D. Haarer, *Nature* **1994**, *371*, 141–143; b) V. Lemaire, D. A. da Silva Filho, V. Coropceanu, M. Lehmann, Y. Geerts, J. Pirijs, M. G. Debije, A. M. van de Craats, K. Senthilkumar, L. D. A. Siebbeles, J. M. Warman, J.-L. Brédas, J. Cornil, *J. Am. Chem. Soc.* **2004**, *126*, 3271–3279.
- I. Seguy, P. Destruel, H. Bock, *Synth. Met.* **2000**, *111*, 15–18.
- J. E. Anthony, *Chem. Rev.* **2006**, *106*, 5028–5048.
- D. J. Vinyard, S. Su, M. M. Richter, *J. Phys. Chem. A* **2008**, *112*, 8529–8533.
- M. T. Cicerone, F. R. Blackburn, M. D. Ediger, *J. Chem. Phys.* **1995**, *102*, 471–479.
- a) Y.-H. Kim, D.-C. Shin, S.-H. Kim, C.-H. Ko, H.-S. Yu, Y.-S. Chae, S.-K. Kwon, *Adv. Mater.* **2001**, *13*, 1690–1693; b) Y. H. Kim, H. C. Jeong, S. H. Kim, K. Yang, S. K. Kwon, *Adv. Funct. Mater.* **2005**, *15*, 1799–1805; c) S. Zheng, J. Shi, *Chem. Mater.* **2001**, *13*, 4405–4407; d) G. Klärner, M. H. Davey, W. D. Chen, J. C. Scott, R. D. Miller, *Adv. Mater.* **1998**, *10*, 993–997; e) J. N. Moorthy, P. Venkatakrisnan, P. Natarajan, D.-F. Huang, T. J. Chow, *J. Am. Chem. Soc.* **2008**, *130*, 17320–17333.
- H. Meng, F. Sun, M. B. Goldfinger, G. D. Jaycox, Z. Li, W. J. Marshall, G. S. Blackman, *J. Am. Chem. Soc.* **2005**, *127*, 2406–2407.
- a) Y.-C. Lin, R. G. Weiss, *Macromolecules* **1987**, *20*, 414–417; b) Y.-C. Lin, R. G. Weiss, *Liq. Cryst.* **1989**, *4*, 367–384; c) S. Norvez, *J. Org. Chem.* **1993**, *58*, 2414–2418; d) S. Méry, D. Haristoy, J.-F. Nicoud, D. Guillon, H. Monobe, Y. Shimizu, *J. Mater. Chem.* **2003**, *13*, 1622–1630; e) S. Norvez, F.-G. Tournilhac, P. Bassoul, P. Herson, *Chem. Mater.* **2001**, *13*, 2552–2561; f) R. Rosenhauer, Th. Fischer, J. Stumpe, R. Giménez, M. Piñol, J. L. Serrano, A. Viñuales, D. Broer, *Macromolecules* **2005**, *38*, 2213–2222; g) R. Giménez, M. Piñol, J. L. Serrano, *Chem. Mater.* **2004**, *16*, 1377–1383.
- a) C. F. J. Faul, M. Antonietti, *Chem. Eur. J.* **2002**, *8*, 2764–2768; b) C. F. J. Faul, M. Antonietti, *Adv. Mater.* **2003**, *15*, 673–683.
- F. Camerel, C. F. J. Faul, *Chem. Commun.* **2003**, 1958–1959.
- a) D. Franke, M. Vos, M. Antonietti, N. A. J. M. Sommerdijk, C. F. J. Faul, *Chem. Mater.* **2006**, *18*, 1839–1847; b) D. Ganeva, M. Antonietti, C. F. J. Faul, R. Sanderson, *Langmuir* **2003**, *19*, 6561–6565; c) A. G. Cook, U. Baumeister, C. Tschierske, *J. Mater. Chem.* **2005**, *15*, 1708–1721; d) W. Li, W. Bu, H. Li, L. Wu, M. Li, *Chem. Commun.* **2005**, 3785–3787; e) M. Marcos, R. Martín-Rapún, A.

- Omenat, J. Barberá, J. L. Serrano, *Chem. Mater.* **2006**, *18*, 1206–1212; f) J. H. Cameron, A. Facher, G. Lattermann, S. Diele, *Adv. Mater.* **1997**, *9*, 398–403; g) D. Franke, C. C. Egger, B. Smarsly, C. F. J. Faul, G. J. T. Tiddy, *Langmuir* **2005**, *21*, 2704–2712.
- [14] F. Camerel, G. Ulrich, J. Barbera, R. Ziessel, *Chem. Eur. J.* **2007**, *13*, 2189–2200.
- [15] M. Yoshio, T. Mukai, H. Ohno, T. Kato, *J. Am. Chem. Soc.* **2004**, *126*, 994–995.
- [16] M. F. Acquavella, M. E. Evans, S. W. Farragher, C. J. Névoret, C. J. Abelt, *J. Org. Chem.* **1994**, *59*, 2894–2897.
- [17] Y. Mizobe, N. Tohnai, M. Miyata, Y. Hasegawa, *Chem. Commun.* **2005**, 1839–1841.
- [18] J. Olmsted, *J. Phys. Chem.* **1979**, *83*, 2581–2584.
- [19] J. Dhote, K. P. Kretsch, A. P. Davey, W. Blau, H. J. Byrne, *Synth. Met.* **1999**, *102*, 1529–1530.
- [20] The absence of the (110) reflection is not infrequent in X-ray patterns of hexagonal columnar mesophases and it is due to a minimum in the form factor, which precludes the observation of peaks at this diffraction angle. For examples, see the following references: a) B. Kohne, K. Praefcke, W. Stephan, *Chimia* **1986**, *40*, 14–15; b) H. Strzelecka, C. Jallabert, M. Veber, P. Davidson, A. M. Levelut, *Mol. Cryst. Liq. Cryst.* **1988**, *161*, 395–401; c) J. Barberá, C. Cativiela, J. L. Serrano, M. M. Zurbano, *Adv. Mater.* **1991**, *3*, 602–605; d) H. Zheng, B. Xu, T. M. Swager, *Chem. Mater.* **1996**, *8*, 907–911; e) J. Barberá, M. Bardají, J. Jiménez, A. Laguna, M. P. Martínez, L. Oriol, J. L. Serrano, I. Zaragoza, *J. Am. Chem. Soc.* **2005**, *127*, 8994–9002.
- [21] F. Camerel, J. Barbera, J. Otsuki, T. Tokimoto, Y. Shimazaki, L.-Y. Chen, S.-H. Liu, M.-S. Lin, C.-C. Wu, R. Ziessel, *Adv. Mater.* **2008**, *20*, 3462–3467.
- [22] a) F. Morale, R. W. Date, D. Guillon, D. W. Bruce, R. L. Finn, C. Wilson, A. J. Blake, M. Schröder, B. Donnio, *Chem. Eur. J.* **2003**, *9*, 2484–2501; b) B. Donnio, B. Heinrich, H. Allouchi, J. Kain, S. Diele, D. Guillon and D. W. Bruce, *J. Am. Chem. Soc.* **2004**, *126*, 15258–15268.
- [23] A. K. Dutta, *Langmuir* **1997**, *13*, 5678–5684.
- [24] a) F. Placin, J.-P. Desvergne, C. Belin, T. Buffeteau, B. Desbat, L. Ducasse, J.-C. Lasségues, *Langmuir* **2003**, *19*, 4563–4572; b) Q. Lü, M. H. Liu, *Chin. Chem. Lett.* **2001**, *12*, 1105–1108.
- [25] a) F. Camerel, L. Bonardi, M. Schmutz, R. Ziessel, *J. Am. Chem. Soc.* **2006**, *128*, 4548–4549; b) F. Camerel, L. Bonardi, G. Ulrich, L. Charbonniere, B. Donnio, C. Bourgoigne, D. Guillon, P. Retailleau, R. Ziessel, *Chem. Mater.* **2006**, *18*, 5009–5021.

Received: March 19, 2009  
Published online: July 11, 2009